#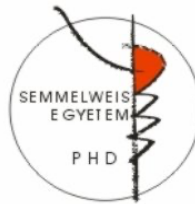 ADVANCES IN MAGNETIC RESONANCE IMAGING OF PERIPHERAL ARTERIAL DISEASE: NON-CONTRAST MAGNETIC RESONANCE ANGIOGRAPHY AND ARTIFICIAL INTELLIGENCE-AIDED PLAQUE ANALYSIS

PhD thesis (short version)

Judit Csőre MD

Cardiovascular Medicine and Research Division
Semmelweis University Doctoral School

Supervisor: Csaba Csobay-Novák, MD, PhD
Official reviewers: Andrea Trajtler, MD, PhD
                         Márton Tibor Berczeli, MD, PhD
Head of the Complex Examination Committee:
                         Tivadar Tulassay, MD, DSc
Members of the Complex Examination Committee:
                         Henriette Farkas MD, DSc
                         Charaf Hassan, DSc

Budapest
2024

1. Introduction

Lower extremity peripheral arterial disease (PAD) is an atherosclerotic condition that causes inadequate blood supply and ischemia to the affected limb. PAD, despite its growing prevalence, mortality, and serious clinical outcomes, is still underdiagnosed and underrecognized. In 2013, approximately 202 million people worldwide lived with PAD, and following coronary artery disease and stroke, it is the third leading cause of atherosclerotic morbidity. To ensure precise treatment planning, non-invasive and invasive imaging techniques are essential. Individuals with diabetes and accompanying renal failure are at an elevated risk for PAD, underscoring the importance of employing nephroprotective imaging techniques for diagnosis. Despite the inherently invasive nature and significant limitations, digital subtraction angiography (DSA) using iodinated contrast material remains the gold standard for imaging of PAD. As an alternative, carbon dioxide (CO_2) DSA can be utilized in those with contrast material sensitivity or impaired renal function. In recent decades, magnetic resonance imaging (MRI) techniques have undergone significant advancements in imaging peripheral arteries, offering several advantages, including the absence of ionizing radiation and the elimination of the need for contrast materials. A novel magnetic resonance angiography (MRA) sequence called Quiescent-Interval Single-Shot (QISS) MRA is a promising technique for lower extremity peripheral arterial imaging both in 1.5T and 3T.

Due to its minimally invasive approach and low periprocedural complication rate, percutaneous vascular intervention (PVI) is often chosen as the initial treatment for PAD. Nevertheless, about 15-30% of patients experience immediate PVI failure, typically attributed to impenetrable plaques. Recent advancements in ultrashort echo time (UTE) MRI sequences have addressed this

1

limitation. UTE sequences are capable of separating calcium from other tissues based on their distinct T2 relaxation time properties. With the use of these state-of-the-art MRI sequences, lesions composed of "hard" (dense collagen and calcium) and "soft" tissue (loose fibrous tissue, microchannels, fat, thrombus) can easily be identified, showing calcium as hypointense, dense collagen as isointense and soft tissue as hyperintense relative to smooth muscle tissue signal. These innovative techniques in MRI are powerful, but their adoption in different clinical setups may be limited due to their complexity in interpretation for untrained physicians. AI-assisted algorithms could potentially facilitate the interpretation process. Widely employed AI algorithms like variational autoencoders (VAEs) offer the advantage of rapid and automated classification once they have been adequately trained.

2. Objectives
As of June 2020, QISS MRA has been introduced at the Semmelweis University Heart and Vascular Center, marking its first availability in Hungary. Over the past few years, we aimed to evaluate the diagnostic effectiveness of this MRA protocol compared to CO_2 DSA and to DSA using iodinated contrast material.

At the Houston Methodist Hospital, (Houston, Texas, USA) we conducted a proof-of-concept study, with the objective of evaluating the feasibility of employing a custom-made VAE using two-dimensional (2D) convolutional neural networks (CNNs) on images obtained from PAD lesions. Our aim was to establish a semi-automated classification of these lesions using a specialized, high-resolution 7T MRI histology protocol that incorporates UTE, T1-wieghted (T1w), and T2-weighted (T2w) contrasts.

3. Methods
3.1. Comparison of invasive imaging methods and QISS MRA
3.1.1. Study design and patient population
Our research was conducted at the Semmelweis University Heart and Vascular Center between June and December of 2020. Individuals with chronic lower extremity PAD who underwent diagnostic DSA were prospectively enrolled and were scheduled to undergo an additional QISS MRA on the day of their DSA. Indication of lower extremity DSA was at the discretion of the primary physician (vascular surgeon or angiologist) and was independent of this current study. In all cases, the investigators were blinded to the reports and the clinical findings of the patient. This single-center study was approved by the local and national ethical committees (registration number: OGYEI/7984/2020).

3.1.2. Imaging protocol
3.1.2.1. DSA using CO_2 and iodinated contrast material
For all patients undergoing diagnostic lower extremity CO_2 DSA, transradial access was employed. Both CO_2 and iodinated contrast examinations were conducted by placing a 4F pigtail/flush catheter into the terminal aorta. As a standard practice, we performed non-selective contrast injection without table tilting. The decision to use selective injection was at the discretion of the interventional radiologist/vascular surgeon and was only performed when non-selective images were deemed insufficient for treatment planning. An automated injector (Angiodroid, Angiodroid SRL, Bologna, Italy) was used for CO_2 delivery. Images were recorded with a modified CO_2 DSA protocol (Siemens Evenflow, 3–4 frames per second (FPS) of a fixed mount imaging system (Siemens Artis Zee, Siemens Healthineers, Erlangen, Germany) with 60 ml injection volume at 500 mmHg injection pressure regardless of region. Iodinated

contrast material (Ultravist 370, Bayer, Germany) was administered using an automated injector (MEDRAD Avanta, Bayer, Germany).

3.1.2.3. QISS MRA protocol

All QISS MRA scans were performed using a 1.5T MR scanner (MAGNETOM Aera, Siemens Healthineers, Erlangen, Germany) in feet first, supine patient positioning. A 36-element peripheral angiographic array coil system was utilized in the lower limb region, supplemented with two 18-element torso coils in the abdominal and pelvic regions. QISS MRA scans were acquired in 9-10 steps in transversal plane with fat saturation and venous suppression, starting from the toes and extending to the abdominal aorta. Electrocardiographic gating was employed for all scans in free breathing in the lower extremity and pelvic regions and in breath-hold in the upper abdominal region. Using the acquired transversal plane images, we generated 3D, rotating, coronal plane MIP reconstructions for all patients.

3.1.3. Image analysis

All CO_2 DSA and QISS MRA images were independently evaluated by two radiologists with ten and four years of expertise in cardiovascular imaging, during individual sessions. Iodinated contrast images were further evaluated by two radiologists, with 5 and 10 years of expertise in PVIs.

Image quality and stenosis grading were assessed for 19 segments as follows: 1—aorta, 2 and 3—bilateral common iliac artery, 4 and 5 —bilateral external iliac artery, 6 and 7—bilateral common femoral artery, 8 and 9—bilateral superficial femoral artery and popliteal artery, 10 and 11—bilateral deep femoral artery, 12 and 13—bilateral tibioperoneal trunk, 14 and 15—bilateral anterior tibial artery, 16 and 17—bilateral posterior tibial artery, 18 and 19—bilateral peroneal artery. Segments that were either not

imaged or only partially imaged, as determined by at least one reviewer, were excluded from the analysis.

Image quality was evaluated using 5-point Likert scale for each segment: 1—non-diagnostic, image quality inadequate for diagnosis; 2—fair, image quality marginally acceptable for diagnosis; 3—moderate, image quality acceptable for diagnosis; 4—good, image quality adequate for confident diagnosis and 5—excellent, excellent image quality providing a highly confident diagnosis. Stenoses were categorized into four classes: no visible stenosis, degree of stenosis <50%, 50–70%, and >70%. In segments with multiple lesions, the most severe stenosis was recorded. For statistical analysis, in cases with discrepancies or uncertainties, final values for both image quality and stenosis were determined through consensus reached by the readers. Subsequently, we divided the segments into three distinct anatomical regions (aortoiliac, femoropopliteal, and tibioperoneal) for the final evaluation.

3.1.4. Statistical analysis

Categorical data were presented as frequencies and percentages, while continuous data were expressed as median and interquartile range (IQR). We used Wilcoxon matched-pair test for the comparison of Likert scores. The degree of inter-rater reproducibility was measured by using intra-class correlation coefficient (ICC). Levels of reliability were as follows: poor, ICC < 0.50; moderate, ICC = 0.5–0.74; good, ICC = 0.75–0.90; excellent, ICC > 0.90). The interpretability of both QISS MRA and DSA was assessed by determining the proportion of non-diagnostic segments among all segments, where a Likert score of 2 to 5 was considered as an image quality adequate for diagnosis. Diagnostic accuracy of QISS MRA in detecting obstructive luminal stenosis (>70%) was evaluated on a per-region basis, with

5

CO_2 DSA and iodinated contrast DSA serving as the reference standard. Statistical significance was defined as a two-sided p-value <0.05 for all analyses. All calculations were performed using SPSS (version 25.0, Armonk, NY, USA).

3.2. Artificial intelligence-aided PAD plaque analysis

This single-center study was carried out in Houston Methodist Hospital, Texas, USA, and was approved by the Institutional Review Board (protocol number: PRO00027258).

3.2.1. High-resolution MRI of amputated limbs

Lower limbs from five patients who underwent major amputation were collected immediately after surgery. Amputation was indicated in cases of end-stage chronic limb ischemia, a decision independent of the current study. Legs then were imaged using an FDA-approved 7T MRI scanner (MAGNETOM Terra, Siemens Healthineers, Erlangen, Germany) equipped with a single-transmit 28-channel knee coil, imitating a clinical setup (feet first-supine position). The MRI protocol included sagittally acquired UTE, T1-weighted (T2w), and T2-weighted (T2w) sequences.

3.2.2. Image preprocessing

T1w, T2w and UTE image contrasts were co-registered using the General Registration module in 3D Slicer software. The aligned volumes were then imported into ImageJ software. To equalize image contrasts, images were normalized across all lesions. Normalized images for the three contrasts (T1w, T2w, and UTE) were combined to create pseudo red-green-blue (RGB) images. The T1w images were assigned as the red component, the T2w images as the green component, and the UTE images as the blue component. Each PAD lesion was manually outlined in the acquired sagittal orientation. The outlined volumes were then resliced with the original resolution to generate axial MPR

reconstructions. Each axial slice was resized to 64x64 pixels. To extract hard/soft components (i.e. dark blue/black and blue, respectively), pixels with hexadecimal RGB values ranging from 0x800000 to 0xff0000 were removed.

3.2.3. Variational autoencoder

Two 2D convolutional neural networks were developed, with the pre-processed images serving as input for the first network. Starting with a 2D input layer comprising three channels for the pseudo-color RGB images, we constructed five convolutional layers with increasing depth. The final layer, the output layer, was flat fully connected with the same number of elements as the last convolutional layer. This output layer was fed into two separate layers: the mean layer and the variance layer. Both of these layers were of the same dimension (2D) as the latent space and represented the mean and variance for two Gaussian distributions. Using these mean and variance values, the representation of each image was calculated based on its coordinates (x and y component) in latent space. The VAE model was implemented on a MacBook Pro (Apple Inc., Cupertino, CA, USA) equipped with the M1 chip, utilizing TensorFlow (version 2.7.0, Google, Mountain View, CA, USA) in Python (version 3.9.9, Python Software Foundation, Austin, TX, USA) with a virtual environment created with Conda (version 4.11.0, Anaconda Inc., Austin, TX, USA). The TensorFlow-Metal Pluggable Device (version 0.8.0, Mountain View, CA, USA) was implemented to allow the use of the Apple M1 Graphics Processing Unit (GPU) approximately accelerate computations by an order of magnitude. With a total of 500 epochs, batch size of 128 and a learning rate of 0.0005 (Adam optimizer) the VAE was trained.

3.2.4. Tissue Classes and latent space classification

By examining the reconstructed black/blue axial luminal cross-sections in latent space, we visually divided this space into four regions, each representing a tissue class associated with PAD. Each tissue class was assigned a numerical tissue score as follows: Tissue Class 1: lumen patent, tissue score 0; Tissue Class 2: lumen partially patent, tissue score 1; Tissue Class 3: lumen mostly occluded soft tissue, tissue score 3 and Tissue Class 4: lumen mostly occluded hard tissue, tissue score 5. To determine the overall tissue characteristics of each lesion sample, an average tissue score was calculated by averaging the tissue scores assigned to each cross-section within the lesion. Additionally, the relative percentages of each tissue class were determined to provide insights into the composition of the lesion.

4. Results
4.1. Comparison of invasive imaging methods and QISS MRA
4.1.1. Comparison of CO_2 DSA and QISS MRA

A total of 28 patients (11 male, mean age 71 ± 9 years) were included in our study, resulting in a total of 523 segments included in the final evaluation, assessed across 164 prioritized regions (aortoiliac, femoropopliteal and tibioperoneal).

4.1.1.1. Image quality

QISS MRA outperformed CO_2 DSA in terms of image quality across all regions. QISS MRA consistently demonstrated a median of good image quality in all cases. The majority of CO_2 angiographies exhibited only a median of moderate image quality, with the femoropopliteal region presenting a median of good image quality (QISS MRA vs. CO_2 DSA; all regions: 4 [4-5] vs. 3 [3-4]; aortoiliac region: 4 [4-5] vs. 3 [3-4]; femoropopliteal region: 4 [4-5] vs. 4 [3-4]; tibioperoneal region: 4 [4-5] vs. 3 [2-3]; all p<0.001) (Figure 1).
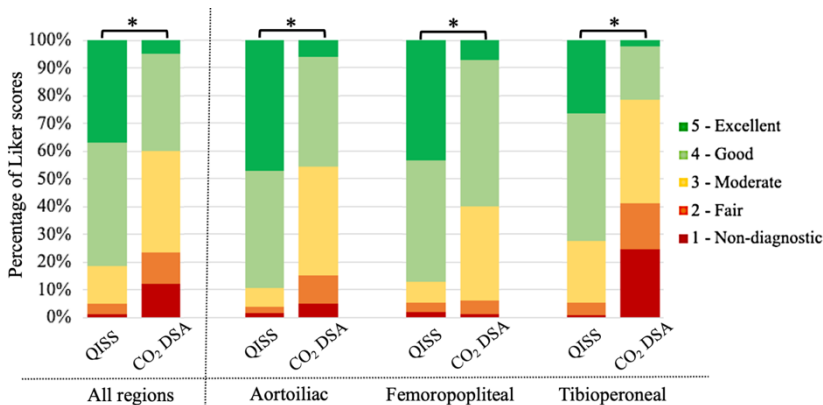
Figure 1: Per-region comparison of Likert scores in subjective image quality assessment of QISS MRA and CO_2 DSA datasets. (DSA: digital subtraction angiography, QISS MRA: Quiescent-Interval Single-Shot Magnetic Resonance Angiography)

4.1.1.2. Diagnostic accuracy

The diagnostic accuracy of QISS MRA was assessed for significant (>70%) stenosis using sensitivity, specificity, positive predictive value (PPV), negative predictive value (NPV), and diagnostic accuracy, with CO_2 DSA serving as the reference standard. The results are as follows: sensitivity 82.6% [95% CI, 74.1-89.2%], specificity 96.9% [95% CI, 94.6-98.5%], PPV 89.1% [95% CI, 82.0-93.6%], NPV 94.8% [95% CI, 91.0-95.6%], and diagnostic accuracy 93.6% [95% CI, 91.0-95.6%].

4.1.1.3. Interpretability

A comparison of the percentage of segments providing adequate diagnostic image quality showed that for all regions combined, interpretability is superior with QISS MRA compared to CO_2 DSA (98.3% vs 86.2%; p<0.001). In the tibioperoneal region, the difference between the two modalities was even more pronounced: 99.1% of QISS MRA images had an image quality

9

adequate for diagnosis, whereas for CO_2 DSA this value was only 71.7% (n/N=221/223vs. n/N=160/223, respectively; p<0.001).

4.1.1.4. Reproducibility

QISS MRA also demonstrated superior performance in the classification of stenoses: inter-observer agreement showed better reproducibility for QISS MRA than CO_2 DSA in all examined regions. The interobserver ICC for QISS MRA was 0.97 for all regions, 0.95 for the aortoiliac region, 0.97 for femoropopliteal region, 0.97 for tibioperoneal region. In contrast, ICC values for CO_2 DSA were 0.81, 0.80, 0.85 and 0.78 for the corresponding regions, respectively.

4.1.2. Comparison of iodinated contrast material DSA and QISS MRA

We evaluated a total of 623 segments from 34 patients (24 men, mean age 67±5 years) across 208 prioritized regions.

4.1.2.1. Image quality

Following consensus assessment, our results indicated that QISS MRA yielded significantly better subjective image quality than DSA for all regions combined and for the below-the-knee region (QISS vs. DSA; all regions: 4 [4-5] vs. 4 [3-5]; tibioperoneal region: 4 [4-5] vs. 3.5 [3-4], both p<0.001). In the aortoiliac and femoropopliteal regions, QISS MRA provided a median of good image quality, comparable to DSA, however, DSA outperformed QISS MRA (aortoiliac region: 4 [4-4] vs. 4 [4-5], p<0.001; femoropopliteal region: 4 [4-4] vs. 4 [4-5], respectively, p=0.01) (Figure 2).
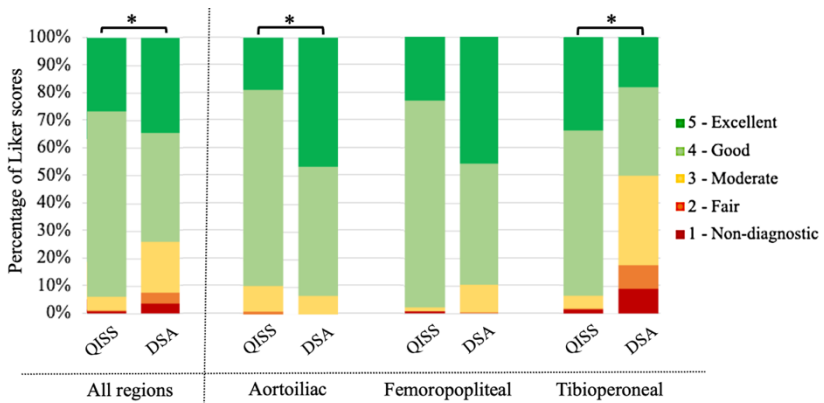
Figure 2: Per-region comparison of Likert scores in subjective image quality assessment of QISS MRA and iodinated contrast DSA images. (DSA: digital subtraction angiography, QISS MRA: Quiescent-Interval Single-Shot Magnetic Resonance Angiography)

4.1.2.2. Diagnostic accuracy

The diagnostic accuracy of QISS MRA in detecting significant (>70%) stenosis was calculated using iodinated contrast DSA as the reference standard, yielding a sensitivity of 84.8% [95% CI, 77.3-90.6], specificity of 93.0% [95% CI, 90.3-95.1], PPV of 76.3% [95% CI, 69.6-81.8], NPV of 95.8%, and diagnostic accuracy of 91.3% [95% CI, 88.7-93.4].

4.1.2.3. Interpretability

Significant interpretability differences were observed between the two modalities across all regions. QISS MRA displayed superior image quality, with only 1% of segments (6/623) deemed non-diagnostic, compared to 3.9% (24/623) with DSA (p<0.001). Particularly in the below-the-knee area, QISS MRA performed even better, with only 0.6% (4/623) segments showing unsatisfactory image quality, while DSA had 9.1% (24/623) non-diagnostic segments, six times higher than QISS MRA (p<0.001).

4.1.2.4. Reproducibility

For stenosis assessment, inter-rater ICC indicated superior agreement between observers for QISS MRA (QISS MRA vs. DSA: all regions: 0.94 [95% CI, 0.93-0.95] vs. 0.88 [95% CI, 0.86-0.90], aortoiliac: 0.91 [95% CI, 0.87-0.93] vs. 0.79 [95% CI, 0.71-0.84], femoropopliteal: 0.92 [95% CI, 0.89-0.94] vs. 0.90 [95% CI, 0.87-0.93], tibioperoneal: 0.95 [95% CI, 0.94-0.97] vs. 0.86 [95% CI, 0.81-0.89]).

4.2. Artificial intelligence-aided PAD plaque analysis
4.2.1. Image preprocessing

A total of 2390 MPR images were obtained from the original five lesion samples, with the distribution as follows: Sample #1: 168 images, Sample #2: 453 images, Sample #3: 943 images, Sample #4: 514 images, and Sample #5: 312 images. To enhance visual representation, pseudo-colors were assigned to different components based on the MRI contrasts used. The arterial wall was represented by red/pink, the free lumen/blood by green, calcium by black, collagen by dark blue, and soft tissue by bright blue. By removing the RGB pixels as described in Methods section, the remaining pixels represented the hard and soft tissues, appearing as black/dark blue and bright blue, respectively (Fig 3).

4.2.2. Variational Autoencoder

Upon visual inspection, the comparison between the original images and the AI-reconstructed pseudo-color images revealed a high level of agreement, indicating successful implementation of the trained 2D CNN VAE. The colors and their spatial distribution in the reconstructed images closely matched those of the original images, with only slight blurring observed in the reconstructed axial slices. Based on the distribution of the reconstructed axial slices in the latent space, the space was

divided into four distinct regions, each corresponding to a specific tissue class. The boundaries for these regions were determined by assigning values to the x and y-components in the latent space as follows: Tissue Class 1: lumen patent, x-value < 0.8, y-value < .8; Tissue Class 2: lumen partially patent; x-value < 0.8, y-value > 0.8; Tissue Class 3: lumen mostly occluded soft tissue, x-value > 0.8, y-value ≤ 0.8 and Tissue Class 4: lumen mostly occluded hard tissue, x-value > 0.8 and y-value ≤ 0.8 (Fig 3).
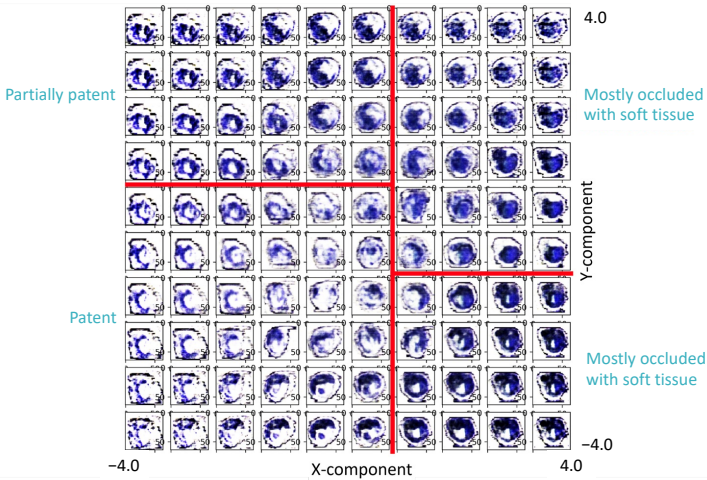

Figure 3: The distribution of reconstructed cross-sections in the latent space is visualized based on the x and y-components. Boundaries are delineated in red to separate the latent space into subregions representing the four tissue classes associated with peripheral artery disease (PAD) lesions. Soft PAD lesion components are depicted in blue/white, while hard components are represented in black.

4.2.3. Tissue scores
Distribution of the tissue scores for the axial slices closely aligned with the visual inspection of each tissue. Tissue scores varied in

range: in lesion sample #1, only Tissue Class 1 was present, indicating a completely patent lumen, with an average tissue score of 0. Lesion sample #3 (average tissue score: 1.06) predominantly featured partially patent regions (Tissue Class 2), with two focal areas showing mostly occluded lumens with soft tissue (Tissue Class 3). Lesion samples #2 (average tissue score 1.33) and #5 (average tissue score 1.44) exhibited similar patterns, with larger regions corresponding to Tissue Class 2 than Tissue Class 3. In lesion sample #4, a significant portion of Tissue Class 4 was surrounded by adjacent Tissue Class 3 regions, resulting in the highest average tissue score observed (2.47). The relative percentages of Tissue Classes for lesion samples #2-#5 demonstrated that Tissue Class 2 had the highest representation, followed by Tissue Class 3 and Tissue Class 1.

5. Conclusions

QISS MRA consistently delivered excellent image quality in comparison to both iodinated and CO_2 contrast DSA, with the highest image quality observed in the tibioperoneal region. Our findings suggest that 1.5T QISS MRA could serve as a valuable alternative for individuals for whom the use of iodinated or gadolinium contrast agents is contraindicated. This non-invasive diagnostic method holds relevance even for patients with normal renal function. By harnessing the potential of this technique, the diagnostic burden on patients can be minimized, potentially leading to earlier disease detection and a reduction in the long-term risk of cardiovascular complications.

In our feasibility study on AI-aided plaque analysis, we demonstrated a novel application of a custom Variational Autoencoder algorithm combined with 2D convolutional networks for analyzing multi-contrast 7T MRI images. Our VAE successfully sorted relevant image features, specifically the

presence or absence of hard and soft tissue types, within the latent space. It is strongly advised and promising for future projects to extend the algorithm and validate its performance using supervised classification techniques. This would bolster the algorithm's capabilities and offer a more thorough assessment of its effectiveness. Additionally, the combination of AI algorithms and MRI histology holds the potential to assist clinicians in personalizing device selection and improving treatment planning.

6. Bibliography of the candidate's publications

Peer reviewed articles with relevance to the current work:
1. **Csőre J**, Suhai FI, Gyánó M, Pataki ÁA, Juhász G, Vecsey-Nagy M, Pál D, Fontanini DM, Bérczi Á, Csobay-Novák C. Quiescent-Interval Single-Shot Magnetic Resonance Angiography May Outperform Carbon-Dioxide Digital Subtraction Angiography in Chronic Lower Extremity Peripheral Arterial Disease. J Clin Med. 2022 Aug 1;11(15):4485. **IF: 3.9**

2. Juhász G, **Csőre J**, Suhai FI, Gyánó M, Pataki Á, Vecsey-Nagy M, Pál D, Fontanini DM, Bérczi Á, Csobay-Novák C. A kontrasztanyag nélküli mágnesesrezonancia-angiográfia diagnosztikus teljesítménye alsó végtagi verőérbetegekben [Diagnostic performance of non-contrast magnetic resonance angiography in patients with lower extremity arterial disease]. Orv Hetil. 2022 Nov 6;163(45):1782-1788. Hungarian. **IF:0.6**

3. **Csore J**, Karmonik C, Wilhoit K, Buckner L, Roy TL. Automatic Classification of Magnetic Resonance Histology of Peripheral Arterial Chronic Total Occlusions Using a Variational Autoencoder: A Feasibility Study. Diagnostics (Basel). 2023 May 31;13(11):1925. **IF: 3.6**

4. **Csore J**, Drake M, Roy TL. Peripheral arterial disease treatment planning using noninvasive and invasive imaging

methods. J Vasc Surg Cases Innov Tech. 2023 Aug 19;9(4):101263. **IF: 0.7**

5. **Csore J**, Roy TL, Wright G, Karmonik C. Unsupervised classification of multi-contrast magnetic resonance histology of peripheral arterial disease lesions using a convolutional variational autoencoder with a Gaussian mixture model in latent space: A technical feasibility study. Comput Med Imaging Graph. 2024 Mar 26;115:102372. **IF: 5.7**

Other peer-reviewed articles:

1. Boga M, Suhai FI, Orbán G, Salló Z, Nagy KV, Szegedi L, Jokkel Z, **Csőre J**, Osztheimer I, Perge P, Gupta D, Merkely B, Gellér L, Szegedi N. Incidence and predictors of stroke and silent cerebral embolism following very high-power short-duration atrial fibrillation ablation. Europace. 2023 Nov 2;25(11):euad327. **IF: 6.1**

2. Fontanini DM, Huber M, Vecsey-Nagy M, Borzsák S, **Csőre J**, Sótonyi P, Csobay-Novák C. Pulsatile Changes of the Aortic Diameter May Be Irrelevant Regarding Endograft Sizing in Patients With Aortic Disease. J Endovasc Ther. 2023 May 8:15266028231172368. **IF: 2.6**

3. Vecsey-Nagy M, Jermendy ÁL, Kolossváry M, Vattay B, Boussoussou M, Suhai FI, Panajotu A, **Csőre J**, Borzsák S, Fontanini DM, Csobay-Novák C, Merkely B, Maurovich-Horvat P, Szilveszter B. Heart Rate-Dependent Degree of Motion Artifacts in Coronary CT Angiography Acquired by a Novel Purpose-Built Cardiac CT Scanner. J Clin Med. 2022 Jul 26;11(15):4336. PMID: 35893427 **IF: 3.9**

4. Simon J, Herczeg S, Borzsák S, **Csőre J**., Kardos AS, Mérges, G, Zsarnóczay E., Szegedi N., Boussoussou M., Vattay B., Kolossváry M, Szilveszter, B, Gellér, L, Merkely B, &

Maurovich-Horvat P. (2022). Extracardiac findings on cardiac computed tomography in patients undergoing atrial fibrillation catheter ablation, Imaging, 14(1), 52-59. **IF: 0.4**

5. Vecsey-Nagy M, Jermendy ÁL, Suhai FI, Panajotu A, **Csőre J**, Borzsák S, Fontanini DM, Kolossváry M, Vattay B, Boussoussou M, Csobay-Novák C, Merkely B, Maurovich-Horvat P, Szilveszter B. Model-based adaptive filter for a dedicated cardiovascular CT scanner: Assessment of image noise, sharpness and quality. Eur J Radiol. 2021 Dec;145:110032. **IF: 4.532**

6. Sarkadi H, **Csőre J**, Veres DS, Szegedi N, Molnár L, Gellér L, Bérczi V, Dósa E. Incidence of and predisposing factors for pseudoaneurysm formation in a high-volume cardiovascular center. PLoS One. 2021 Aug 24;16(8):e0256317. **IF: 3.752**

7. Simon J, Panajotu, A, **Csőre, J**, Pólos, Miklós, Zsarnóczay, Emese, Merkely B, Maurovich-Horvat P. "Anomalous Left Coronary Artery Originating from the Right Coronary Sinus with an Interarterial Course: a Case Report and Literature Review" Journal of Cardiovascular Emergencies, vol.6, no.2, 2020, pp.35-39. **IF: -**

8. Kádár K, **Csőre J**, Liptai Cs, Tóth A, Kovács A, Molnár L, Suhai FI, Assabiny A, Kuthi, L, Édes I, Kertész AB, Merkely B, Hartyánszky I. Kawasaki-betegség gyermekkortól a felnőttkorig. Multimodális képalkotók szerepe a hosszú távú nyomonkövetésben CARDIOLOGIA HUNGARICA 47 : 4 pp. 243-249. , 7 p. (2017) **IF: -**